Results Solution Splitting, 2D cylindrical symmetry, May 2nd

David Pastor

1 Introduction

Different compounds (nutrients, waste, oxygen, etc.) move through the body via the vascular system. This transport inside the vascular system is mostly pressure driven thanks to the pumping action of the heart. The main process by which compounds are transported is advection. Therefore, it is expected that the ratio of $\frac{U_{eff}L}{D_{eff}}$, also known as the Peclet number, will be higher than one.

The problem of solute transport in the brain is given by the PDE system 1. Equation 1a is the effectie transport equation for the vascular system, whose support is one dimensional ($\Lambda \in \mathbb{R}$)

Once a molecule arrives to the brain microvasculature, it may diffuse through the wall of the smaller vessels (i.e. capillaries and arterioles) into the parenchyma, where it diffuses driven by concentration gradients. The modelling of this coupled system formed by the intravascular transport in the brain microvasculature, and the diffusive transport in the brain parenchyma is shown in 1, and will constitute the focus of this text.

$$\frac{\partial \phi}{\partial t} - \nabla \cdot D\nabla\phi = M_t \frac{\phi}{\phi_o + \phi} + q\delta_\Lambda \quad in \quad \Omega \tag{1a}$$

$$\frac{\partial \langle\phi\rangle}{\partial t} = \frac{\partial}{\partial s} D_{eff} \frac{\partial}{\partial s}\langle\phi\rangle - U_{eff}\frac{\partial}{\partial s}\langle\phi\rangle - K_{eff}(\langle\phi\rangle - \bar{\phi}) \quad in \quad \Lambda \tag{1b}$$

$$q(s) = K_{eff}(\langle\phi\rangle - \bar{\phi})\pi R_v^2 \tag{1c}$$

with the definition of delta:

$$\iiint_\Omega q\delta_\lambda dV = \int_\Lambda q ds \tag{2}$$

The different terms used in 1 are given in the following box

Terms:

- ϕ: extravascular scalar field (e.g. concentration) $[kg/m^3]$
- $\langle\phi\rangle$: intravascular scalar field $[kg/m^3]$
- $\bar{\phi}$: Extra vascular value of ϕ at the vessel (in Λ) $[kg/m^3]$
- D_{eff} : Effective diffusion coefficient in the vascular system $[m^2/s]$
- K_{eff}: Effective permeability $[s^{-1}]$
- U_{eff}: Effective advection coefficient [m/s]
- Ω: 3D support of the problem
- Λ: 1D support of the vascular system. Includes the vessels center lines
- M_t: Maximum tissue consumption/creation rate in the Michaelis-Menten equation $[kg/m^3s]$
- ϕ_o: Concentration at which the consumption is half of its maximum $[kg/m^3]$
- δ_λ: Dirac delta function that is zero everywhere except at the vessel center line $[m^-2]$
- $q(s)$: Molecular (coupling) flux being exchanged between the vascular system and the parenchyma. It will be positive if the flux enters the parenchyma. $[kgm^{-1}s^{-1}]$
- R_v: Radius of the vessel [m]
- s: abscissa that parametrizes the vascular system

A crucial feature of this model is the derivation of a general 1-D effective transport equation for the cross-section-averaged concentration inside the vessel developed in [Berg et al., 2019] shown in equation 1b. This allows the support of the vascular system (given by λ) to be reduced to the vessels centerline, thereby simplifying the computation of 1. The parenchyma is treated as a 3 dimensional space where molecules can diffuse. The diffusion coefficient of this medium is assumed to be homogeneous and isotropic.

2 FV formulation

The tissue equation (equation 1a) is generally solved through FV discretization of the tissue volume, given the conservativeness of the numerical scheme. Due to the large dimensions of the reservoirs or brain tissue to the size of the pores, generally, square or polygonal cells are used, since they are rarely designed to match the pore structures (i.e. the vessels).

The finite volume formulation performs integral balances of equation 1a, by transforming the divergence term into flux balance through the cell's enclosing surface.

Equation 1a is reformulated to agree with other models in literature into equation 3:

$$\frac{\partial \phi}{\partial t} + \nabla \cdot \mathbf{j} = q' - M_t f(\phi) \tag{3a}$$

$$q' = \sum_i q_i \delta_{\Lambda_i} \tag{3b}$$

3b is used to represents the sources or sinks of materials from the vascular system as a discrete sum of point (or line, depending on the definition of δ_Λ) sources, which will allow to simplify the formulation to solve 1b substantially.

In the system 3, the transport equation inside the vascular system has been removed in order to focus on the computation of the solution in the 3 dimensional domain. ϕ represents a scalar field, it can be concentration $[kg/m^3]$ in this case, or pressure when working with Darcy's law $[Pa]$. The flux in equation 3, can be calculated through Fick's law in our case:

$$\mathbf{j} = -D\nabla\phi \quad in \quad \Omega \tag{4}$$

where D represents the diffusion coefficient of the medium $[m^2/s]$, ϕ the scalar concentration field, and $\mathbf{j}$ the mass flux per unit surface area $[kgm^{-2}s^{-1}]$

To show the FV formulation for 3 we further simplify the system to a steady state without tissue consumption. Therefore, we obtain a conservative scalar field in ϕ. The sum of discrete sources will be substituted by a single source for the initial model.

$$\nabla \cdot \mathbf{j} = q\delta_\Lambda \tag{5}$$

After integration over a control volume, the following is obtained:

$$\iiint_{CV} \nabla \cdot \mathbf{j} dV^3 = \iiint_{CV} q\delta_\Lambda dV \tag{6}$$

Where dV represents a differential in volume. Through the definition of the delta distribution and the divergence theorem, we obtain:

$$\iint_\Gamma \langle \mathbf{j}, \mathbf{n} \rangle dS = q_\Lambda \tag{7}$$

Γ represents the surface enclosing the control volume (CV), therefore $\langle \mathbf{j}, \mathbf{n} \rangle$ represents the scalar product between the vector field $\mathbf{j}$ and the normal vector of the surface. Additionally dS is the differential of surface area of Γ.

3 Coupling models

The focus in this section is to provide the tools to solve a simplified version of equation 1a through a FV scheme (could easily be written for a FE or FD schemes). The non-linear tissue consumption term found and temporal variations in equation 1a will be neglected in the text. The goal of the text consists in providing the foundations for a coupling model for eqs. 1 suitable for large microvascular networks . After applying these simplifications, We obtain the following PDE:

$$\nabla \cdot D\nabla\phi = -q\delta_{\Lambda} \tag{8}$$

Where D represents a permeability of the medium to the diffusion like process driven by the gradients of the scalar field (ϕ). For reservoirs, the D represents the Darcy permeability for the porous medium (normally represented as K). For diffusion processes, D represents the diffusion coefficient of the medium.

3.1 Peaceman-like formulations

The system 8 is present in multiple physics problems [Peaceman, 1978]. The approach multiple authors have chosen in order to solve similar systems is based in the accurate characterization of the scalar fields surrounding the sources. Since the analytical solution to the Poisson equation around the source is known, the strength of the source can be approximated. Evidences have been shown that the diffusion coefficient in the parenchyma tends to be homogeneous [Holter et al., 2017]. For now, it will be neglected to further simplify eq. 8

$$-\nabla^2\phi = q\delta_{\Lambda} \tag{9}$$

As in [Peaceman, 1978] and many others [Jayasinghe et al., 2019; Koch et al., 2020a,b; Aavatsmark and Klausen, 2003], the field surrounding the source is given by:

$$\phi(\rho) = \phi_w - \frac{q}{2\pi} ln(\frac{r}{r_w}) \tag{10}$$

To be able to calculate the pressure solution through the reservoir via finite differences, the model requires a link between the "block pressure" (i.e. the numerical pressure computed at the cell the well lies on) and the well pressure, more specifically the pressure at the interface between the well and reservoir (in the presence of skin zone it would be the pressure in the interface between the skin zone and the reservoir rock).

The standard in the literature is the approach introduced by [Peaceman, 1978], where an equivalent radius is calculated (numerically) where the numerical so-

lution (generally calculated via finite differences) is equivalent to the analytical expression of the scalar field surrounding the well (given by equation 10).

The key finding in [Peaceman, 1978] is that the "block pressure" is not equivalent to the average pressure inside the block. This is due to the fact that a finite difference scheme models the gradient through the discretized cell using (normally) an approximation with an order of accuracy $O(h^2)$, with h being the cell size. Equation 10 shows how the gradients will not be accurately estimated through a linear approximation, since the profile is logarithmic (therefore the gradients driving the fluxes will be inveresely proportional to the distance to the well). Peaceman arrives at the estimation of the equivalent radius:

$$r_0 \approx 0.2h \tag{11}$$

That way the "block pressure" can be obtained

$$\phi_o = \phi_w - \frac{q}{2\pi} ln(\frac{0.2h}{r_w}) \tag{12}$$

The main shortcommings of this type of coupling are the following:

- Necessity of estimating the well pressure (ϕ) in order to compute the scalar field
- The solution is highly dependent on the well radius (r_w)
- Necessity of computing the equivalent radius (r_0), which is different for each configuration of wells and volume discretization
- The block pressure does not correspond to the average pressure for the block. Does this produce material imbalances? How could we know?
- The calculation of the equivalent radius becomes very complicated with several tortuous vessels inside a single block.

3.2 Analytical coupling function for the scalar field

A common approach to numerically solve the singularity that appears on equation 9 is use an analytical function that solves for the scalar field at a given distance from the source. This approaches stem from the Peaceman well model since they use the analytical solution of equation 8 to model the field in the vicinity [Peyrounette et al., 2018; Jayasinghe et al., 2019; Koch et al., 2020a]. In a very general sense, the essence of the approach is the following:

Taking equation 9, the scalar field surrounding the source is assumed to be:

$$\phi(r) = \phi_w - \frac{q}{2\pi D} ln\Big(\frac{r}{R_v}\Big) \quad in \quad r > R_v \tag{13}$$

Where r represents the distance to the source, ϕ_w the value of the concentration at the vessel wall in the parenchyma, and R_v the radius of the vessel. The next step lies in the definition of the field for $r < R_v$, since equation 13 has a singularity when $r \to 0$. Each research group uses a different coupling function to couple the microscale ϕ-field (intravascular) with the mesoscale ϕ-field (equation 13).

One of the main drawbacks of this formulation is the fact that the assumption that there is an analytical solution for the scalar field in the vicinity of the source, which is not always the case. Furthermore, this formulation, when there are multiple sources close together, assumes the solution of the field can be obtained as the linear superposition of the influence of different sources (i.e. the solution will be correct as long as the operator applied over the unknown ϕ is linear, which is obviously not the case in equation 1a).

The main advantage is the fact that the coupling is solved analytically, therefore the solution in the vicinity of the source will be highly accurate (that is why the Peaceman model is commonly used as validation for other newer models). Therefore, the precission of the model will depend on the numercial scheme used for the meso scale solution (which is commonly a finite volume method due to the conservative nature of the method)

3.3 MSFV

The MSFV method is a general method to solve elliptic problems with several spatial scales arising from flow in porous media. Here, the focus lies in the model developed in [Jenny et al., 2003] due to its popularity and similarity to the problem at hand in 1.

Their model, adapted to the problem shown in 8, would proceed as follows. Given Fick's law for diffusion in a homogeneous medium with isotropic diffusion coefficient, we can obtain the mass flux by equation 4. Furthermore, the domain Ω is partitioned into smaller volumes $\{\Omega_k\}$, a finite volume solution will satisfy:

$$\iiint_{\Omega_k} \nabla \cdot \mathbf{j} dV = \oint_{\partial\Omega_k} \mathbf{j} \cdot \mathbf{n} d\Gamma = - \iiint_{\Omega_k} q(s)\delta_\Lambda dV = - \int_{\Lambda_k} q(s) ds \tag{14}$$

Where Λ_k represents the 1D vessels situated inside of the sub-volume Ω_k, and $\mathbf{n}$ represents the unit normal vector pointing outwardly of the surface $\partial\Omega_k$. The challenge lies in finding a good approximation for $\mathbf{j} \cdot \mathbf{n}$ on $\partial\Omega_k$. In a general manner, the flux is approximated by:

$$\mathbf{j} \cdot \mathbf{n} = \sum_{i \in N} T^i \phi_i \tag{15}$$

Where N represents a neighourhood of k. T^k denotes a transmissibility. The accuracy of the method is strongly linked on the calculation of these transmissi-

bilities. In [Jenny et al., 2003] the transmissibilities are given by a series of basis functions that are obtained from solving the flow problem at the micro-scale in the vicinity of the sources. In order to obtain this basis functions, the grid is refined on the volume around the sources, and the micro-scale flow problem is resolved there.

The advantages and drawbacks of this method are straightforward: the scalar field is highly accurate since it is solved at the microscale level where the large gradients take place. The drawbacks are the much higher computational cost in comparison with the other methods shown here, due to the necessary refinement surrounding the sources. In the brain microvasculature, where there are billions of vessels, this approach by itself would not be feasible.

3.4 Discrete Fracture Modelling

ToDo

3.5 Secomb et al.

ToDo

4 Solution splitting

The ideal characteristics of an approach for solving the PDE system 1 include:

- The numerical model is conservative
- Accurate estimation of the scalar field surrounding the sources/sinks in order to properly estimate the coupling flux (eq 1c)
- Relatively low computational requirements to be able to perform simulations in large networks
- It produces a sparse system, i.e. the balance equations at any point of the domain are local.
- Ability to incorporate the non linear term for the tissue consumption
- Robustness within the regimes that might take place in the brain: Ideally we would be able to model different situations of nutrient transport (e.g. high intravascular concentration with low extravascular concentration) as well as wate removal (low intravascular concentration with high extravascular concentration)

An approach that might provide an acceptable compromise between accuracy and computational requirements while satisfying the robustness, locality of the scheme, and with the ability to incorporate the non-linear term for consumption might be obtained by splitting the solution of the extravascular scalar field into

several terms as commonly done in literature [Ding and Jeannin, 2001; Gjerde et al., 2019].

The current problem is given by the Poisson equation in 16:

$$-D\nabla^2\phi = q\delta_\Lambda \quad in \quad \Omega \tag{16a}$$

$$\phi(\mathbf{x}) = 0 \quad on \quad \partial\Omega_D \tag{16b}$$

$$\nabla\phi(\mathbf{x}) \cdot \mathbf{n} = 0 \quad on \quad \partial\Omega_N \tag{16c}$$

Where $\partial\Omega_D \bigcup \partial\Omega_N = \partial\Omega$ and $\partial\Omega_D \bigcap \partial\Omega_N = \{0\}$

The goal of this section is to provide a well posed problem that will be simulated in the next sections with the purpose of analyzing its performance regarding the ideal requirements of the numerical scheme mentioned above.

The first step would be to split the solution into a regular term and a sinigular one:

$$\phi(\mathbf{x}) = \phi_r(\mathbf{x}) + \phi_s(\mathbf{x}) \tag{17}$$

The goal of the splitting is twofold: Firstly, to remove the singularity from the equation. Secondly, with the deliberate choice of the analytical function for the singular term (ϕ_s), the provided solution might be able to be represented as a linear combination of the perturbation caused by different sources added to a regular term that aims to correct to take into account further sources and the boundary conditions. The following splitting is suggested:

$$\phi_r(\mathbf{x}) = v(\mathbf{x}) \tag{18a}$$

$$\phi_s(\mathbf{r}, s) = \sum_{j \in sources} \mathscr{G}_j(\mathbf{r}) q_j(s) \tag{18b}$$

$$\phi(\mathbf{x}) = v(\mathbf{x}) + \sum_{j \in sources} \mathscr{G}_j(\mathbf{r}) q_j(s) \tag{18c}$$

The splitting above is chosen taking into account the two objectives mentioned above. [1]

Therefore, the $\mathscr{G}$ function is chosen in order to solve for the source shown in 16a. It will be the solution to the following problem:

$$-\nabla^2\mathscr{G} = \delta_\Lambda \quad on \quad \Omega \tag{19}$$

for each source labeled as j. Therefore it corresponds with the infinite domain Green's function of the Poisson equation for each individual source.

[1] There is a mix of coordinate systems, is it necessary to change it so there is a common coordinate system for the two terms?

5 Resolution of the Split Problem

Terminology of the numerical scheme

- FV: Finite Volumes numerical scheme
- Δs: FV cell size in the axial direction$[m]$
- Δr: FV cell size in the radial direction$[m]$
- r_k: radial position of the center of the cell k.
- Θ: discrete laplacian operator applied to the space Ω
- v: regular term, previously called ϕ_r
- $boundary_{inner}$: in eq. 52 represents the vessel wall
- V_{Ω_k}: volume of the finite volume Ω_k

In order to evaluate the solution splitting technique a test problem is developed. The computational domain (Ω) consists in a cylinder of depth L and diameter $2R_{max}$. For simplicity $R_{max} = L$. In order to achieve cylindrical symmetry and perform a 2D simulation the vessel coincides with the axis of the cylinder. With this configuration the source term modelled via the Dirac's delta function (δ_Λ) is substituted by a boundary condition. We obtain the full problem of the concentration field:

$$\Delta\phi = 0 \quad in \quad \Omega \tag{20a}$$

$$\frac{\partial\phi}{\partial s} = 0 \quad on \quad \partial\Omega_{east,west} \tag{20b}$$

$$\phi(R_{max}, s) = 0 \quad on \quad \partial\Omega_{ext} \tag{20c}$$

$$\frac{\partial\phi}{\partial r} = -\frac{1}{2\pi R_v} q \quad on \quad \Omega_{in} \tag{20d}$$

This system is equivalent to the one shown in equation 1, in a steady state configuration and no tissue consumption.

Choosing:

$$\mathscr{G}(r) = -\frac{1}{2\pi D} log(\frac{r}{R_v}) \tag{21}$$

Since the expression for the singular term is already given, the objective of this section is to obtain the well posed problem for the regular term. As well as to be able to write the influx ($q(s)$) in function of the regular term (otherwise the singular term will not be defined) Firstly we calculate the inner boundary condition (BC on the wall of the vessel)

$$\frac{d\mathscr{G}(r)}{dr} = -\frac{1}{2\pi R_v} \quad for \quad r = Rv \tag{22}$$

Therefore, it simplifies the split problem since the inner boundary condition banishes for the regular term:

$$\frac{\partial \phi}{\partial r} = -\frac{1}{2\pi R_v} q = q\frac{d\mathscr{G}(r)}{dr} + \frac{\partial \phi_r}{\partial r} \tag{23}$$

Therefore:

$$\frac{\partial \phi_r}{\partial r} = 0 \quad on \quad \Omega_{in} \tag{24}$$

This is the main reason for the choice of $\mathscr{G}$ in equation 21. [2]

Since the singular term is given analytically, the succesfull resolution for the regular term will provide the solution of the full problem given in 20 (as long as it also provides the correct estimation of $q(s)$).

$$\Delta\phi = \Delta(\mathscr{G}(r)q(s)) + \Delta\phi_r \tag{25}$$

$$-\delta_\Lambda \frac{q}{D} = (\Delta\mathscr{G}(r))q(s) + 2\nabla\mathscr{G} \cdot \nabla q + \mathscr{G}q"(s) + \Delta\phi_r \tag{26}$$

For this particular problem we have:

$$\Delta\phi_r = -\mathscr{G}(r)\frac{d^2q}{ds^2} \tag{27}$$

with the following boundary conditions:

$$\frac{\partial \phi_r}{\partial s} = -\mathscr{G}(r)\frac{\partial q(s)}{\partial s} \quad on \quad \partial\Omega_{east,west} \tag{28}$$

$$\phi_r(R_{max}, s) = -\mathscr{G}(R_{max})q(s) \quad on \quad \partial\Omega_{ext} \tag{29}$$

For the internal boundary conditions (near the vessel wall:

$$\nabla\phi \cdot \mathbf{n} = -\frac{q(s)}{2\pi R_v} \tag{30}$$

For this simple case:

$$\mathbf{n}_{inner} = -\mathbf{e}_r$$

$$\frac{\partial \phi}{\partial r} = \frac{q(s)}{2\pi R_v} \quad on \quad \Omega_{in} \tag{31}$$

Further:

$$\nabla(\mathscr{G}(r)q(s)) \cdot (-\mathbf{e_r}) = \frac{q(s)}{2\pi R_v} \quad on \quad \Omega_{in} \tag{32}$$

[2] for now we keep this notation with $\mathscr{G}$, because after this we will have a source term problem. But for now we have a BVP, and this $\mathscr{G}$ does not represent a Green function.

Therefore:

$$\frac{\partial \phi_r}{\partial r} = 0 \quad on \quad \Omega_{in} \tag{33}$$

Due to the choice of $\mathscr{G}$ shown in 21, we obtain a straight forward expression for equation 1c in function of the intravascular concentration and the regular term:

$$\bar{\phi} = \mathscr{G}(R_v)q(s) + \phi_r(R_v, s) = 0 + \phi_r(R_v, s) = \bar{\phi_r} \tag{34}$$

Thereby obtaining an expresion for the coupling flux in function of the regular term:

$$q(s) = K_{eff}(\langle\phi\rangle - \bar{\phi_r})\pi R_v^2 \tag{35}$$

Finally, we obtain the full problem for the regular term:

$$\Delta\phi_r = -\mathscr{G}(r)\frac{d^2q}{ds^2} \quad in \quad \Omega \tag{36a}$$

$$\frac{\partial \phi_r}{\partial s} = -\mathscr{G}(r)\frac{\partial q(s)}{\partial s} \quad on \quad \partial\Omega_{east,west} \tag{36b}$$

$$\phi_r(R_{max}, s) = -\mathscr{G}(R_{max})q(s) \quad on \quad \partial\Omega_{ext} \tag{36c}$$

$$\frac{\partial \phi_r}{\partial r} = 0 \quad on \quad \Omega_{in} \tag{36d}$$

Notice how the equation for the regular term (RHS of the eq. 36a), this consumption (or creation) term could be added to the tissue consumption term without modification of the numerical scheme. Therefore, the challenge of dealing with the non-linear consumption term might be solved here.

5.1 Numerical scheme for the coupled system

To solve the equation 36a, a conventional FV method in cylindrical coordinates is used. The domain is discretized in smaller elements denominated Ω_k. The unknowns of this problem are the cell's concentration value (ϕ_r in equation 36a) and the coupling flux through the vessel wall (q in equation 35).

For simplicity, the intravascular concentration is given by the variable $\langle\phi\rangle$ by the following expression:

$$\langle\phi\rangle = cos(\frac{s}{0.7 \cdot L})) \tag{37}$$

The initial concentration in tissue is assumed to be zero. Therefore, for the steady state problem:

$$M * \begin{Bmatrix} v \\ q \end{Bmatrix} = \begin{Bmatrix} 0 \\ \langle\phi\rangle \end{Bmatrix} \tag{38}$$

With M given by:

$$M = \begin{bmatrix} [\Theta] & [b] \\ [c] & [d] \end{bmatrix} \tag{39}$$

a change of terminology is used for the regular term and the RHS of eq. 36a:

$$v = \phi_r \tag{40}$$

$$\Delta v = -F \quad in \quad \Omega \tag{41}$$

$$F = \mathscr{G}(r)\frac{d^2q}{ds^2} \tag{42}$$

Θ represents the discrete operator of the laplacian inside of the domain minus the boundary fluxes (that depend on the boundary conditions).

$$\Theta(v) \approx \frac{\iiint_{\Omega_k} \nabla^2 v dV - \oiint_{\partial\Omega_k} \nabla_n v dS}{V_{\Omega_k}} \tag{43}$$

$$\oint_{\partial\Omega_k} \nabla_n v dS = \oint_{east,west} \nabla_n v dS \tag{44}$$

Therefore:

$$\Theta(v) \approx \frac{\iiint_{\Omega_k} -F dV + \iint_{east} \mathscr{G}(r)\frac{\partial q(s=L)}{\partial s} dS - \iint_{west} \mathscr{G}(r)\frac{\partial q(s=0)}{\partial s} dS}{V_{\Omega_k}} \tag{45}$$

Given a homogeneous discretization size of a cell k: $\Delta s, \Delta r$, together with the cylindrical symmetry allow for the simplification of the above integrals:

$$\Theta(v) \approx \frac{2\pi \int_{r_k} -\mathscr{G}(r) r dr \int_{s_k} \frac{d^2q}{ds^2} ds + 2\pi \frac{\partial q(s=L)}{\partial s} \int_{r_k} \mathscr{G}(r) r dr}{2\pi r_k \Delta r \Delta s} \tag{46}$$

$$\Theta(v) \approx \frac{-\int_{s_k} \frac{d^2q}{ds^2} ds + \frac{\partial q(s=L)}{\partial s}}{r_k \Delta r \Delta s} \int_{r_k} \mathscr{G}(r) r dr \tag{47}$$

For the east boundary conditions

Therefore, for the numerical scheme:

$$M = \begin{bmatrix} [\Theta] & [b] \\ [c] & [d] \end{bmatrix} \tag{48}$$

with:

$$[a] = \Theta \tag{49}$$

$$[b] = \frac{\int_{s_k} \frac{d^2q}{ds^2} ds \pm \frac{\partial q(s = west, east)}{\partial s}}{r_k \Delta r \Delta s} \int_{r_k} \mathscr{G}(r) r dr \tag{50}$$

To assemble the lower part of the matrix M:

$$[c] * v + [d] * q = \langle \phi \rangle \tag{51}$$

$$v(bouundary_{inner}) + \frac{1}{K_{eff} \pi R v^2} q = \langle \phi \rangle \tag{52}$$

$$M = \begin{bmatrix} [\Theta] & \left[\frac{\int_{s_k} \frac{d^2q}{ds^2} ds \pm \frac{\partial q(s = west, east)}{\partial s}}{r_k \Delta r \Delta s} \int_{r_k} \mathscr{G}(r) r dr \right] \\ [Id] & \left[\frac{1}{K_{eff} \pi R v^2} \right] \end{bmatrix} \tag{53}$$

and the full stationary problem:

$$M * \begin{Bmatrix} v \\ q \end{Bmatrix} = \begin{Bmatrix} 0 \\ \langle \phi \rangle \end{Bmatrix} \tag{54}$$

Important topics:

- The following example shows the comparison between: a fine numerical solution used as validation, a solution splitting with very coarse grid, and a coarser solution with a standard FV numerical scheme. Each solution is denominated as: validation, 50x50 and Solution split respectively

- The resolution of each domain is 150x150 (FV validation), 5x5 (Sol Split), 50x50 (FV reference) FV cells respectively.

- The discretization of the vessel is the same for all three solutions! 150 cells per vessel

- Due to the different resolution of the domain there are challenges when comparing the solutions! Interpolation and local averaging will be needed to do for some comparisons

Case	grid size	numerical scheme	name in plots
Validation	150x150	FV conventional	Validation
Reference	50x50	FV conventional	50x50 numerical
Sol Split	5x5	section 5.1	Sol Split

Table 1: Cases used in the simulation to evaluate the performance of the coupling model developed in section 5

6 Results

6.1 Evaluation of the Split solution with the Validation: 5x5 vs 150x150

As previously mentioned in section 3, there are several characteristics desired in a coupling model developed in sections 8 and 5. In this section, focus will be drawn to analyze the accuracy, and the computational efficiency of the model. Firstly, in order to evaluate the accuracy, the Split solution is compared with a reference solution, which is computed via a conservative FV volume approach, with a refined grid (150 x 150 gridcells). In order to evaluate the computational efficiency the solution is compared with a 50 x 50 grid solution solved through the same FV approach. The 50 x 50 solution is meant to mimic the local refinement that would appear in the MSFV approach shown in section 3. As a summary, three solutions will be shown in the section: a 150x150 grid FV reference solution used as validation, a 50x50 grid FV solution used for comparison, and a 5X5 grid solution Split solution where FV method was used to solved the PDE system shown in **??** (see also table 1). Furthermore, the intravascular network (i.e. the vessel) is discretized in 150 cells in the three cases. Therefore, the only differences between the cases arrive in the tissue domain. The averaged vessel concentration is given for all cases as shown in equation 37.

In figure 1 we can see the comparison between the reference solution and the solution split. The large gradients near the vessel wall are not seen in the plot due to the lower resolution that is obtained through the 5x5 grid. The radial variation in of the concentration profile are shown in figure 2 down, where it is clear that the radial gradients that other numerical schemes such as FV or FEM have a difficult time capturing, when taking advantage of the singular term as shown in section 5, these gradients are captured with great accuracy for the whole domain. Furthermore, in the axial plots, shown as well in figure 2 there is great agreement between the two solutions. However, there is a clear deviance from the ideal solution near the exterior and east boundaries. This is due to the boundary effects due to the flux imposition, which is greatly accentuated with coarse grids such as this case.

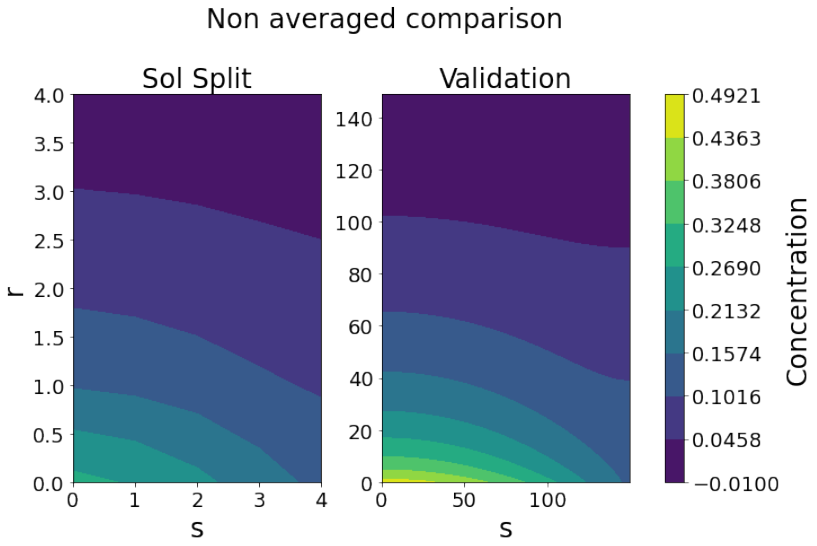

Figure 1: Contour of the scalar field ϕ through solving the regular term with regular FV scheme. The purpose of this plot is to show the lack of distortion of the ϕ-field far from the vessel

6.2 Evaluation of the Sol Split in comparison with the Reference numerical solution: 5x5 vs 50x50 (vs 150x150)

The challenge of a coupling model lies in obtaining a higher accuracy or lower computational expense (or both) than the "gold standard" MSFV presented in section 3.3. This is the reason of the introduction of the 50x50 FV solution, which is intended to mimic the grid refinement near the vessel wall, with the purpose of accurately capturing the large radial gradients. Since the FV scheme is conservative, the interest in modeling the radial gradients is not necessarily to provide an accurate description of the micro-scale concentration field, but to provide a proper estimation of the tissue concentration at the vessel wall in order to properly estimate the inlet flux through equation 1c or 35.

The inlet flux estimation is shown in figure 3, where it can be seen the solution splitting provides an slightly better estimation of the flux, therefore, obtaining a better estimation of the quantity of matter in tissue. An important deviation takes place in the solution split case near the east boundary (end of plot figure 3 and 4). The reason for this probably lies in the treatment of the east boundary and the nature of the regular term. In order to provide an accurate estimation of the coupling flux through the solution splitting technique interpolation is needed (linear in this case) for the regular term, which represents the $\bar{\phi}$ of equation 1c through equation 5. This interpolation is made through an inverse relationship to the distance to the neighboring cells, which there are none in the boundary. Therefore, there is a great loss of accuracy near the east boundary

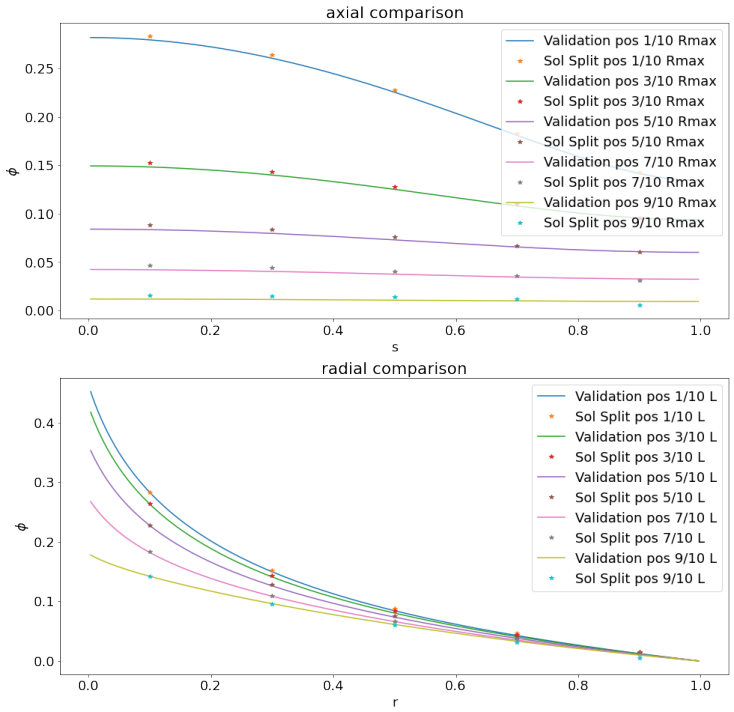

Figure 2: comparison of the concentration profile along different straight lines. The comparison is made between the validation (reference) and the solution split (sol split). In the higher figure, the axial profiles for 5 equidistant radial positions are shown. In the legend, the radial position with respect to the maximal radius is shown for each profile plotted. In the lower figures the radial profiles are shown for 5 equidistant axial positions.

due to the lack of a east cell to interpolate. Additionally due to the nature of the concentration profile chosen in equation 37, the most rapid variation takes place near the eastern boundary, which further pollutes the results. This loss of accuracy can be avoided with a proper interpolation scheme near the boundaries, moreover, this will not pollute the overall result due to the fact, that normally, there are adjacent cells to the ones that contain vessels.

This effect is clearly seen when observing the comparison between the calculated $\bar{\phi}$ in figure 3. The concentration near the west boundary is properly estimated due to the slow variation of the intravascular concentration, which is the opposite case in the east boundary. This is seen as well in figure 4, where the error shots up near the boundary for both solutions. In the case of the 50x50 solution, this error is smaller due to the lower influence of boundary effects on smaller grids.

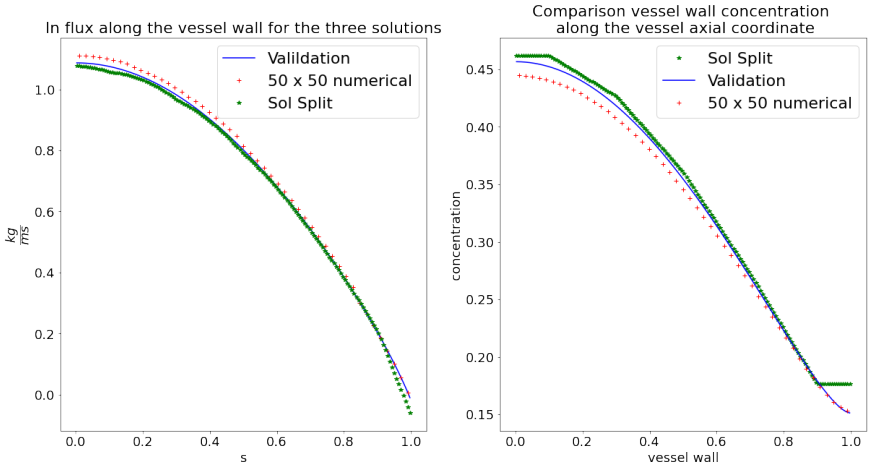

Figure 3: Comparison of the performance of the schemes in predicting in flux and vessel wall concentration

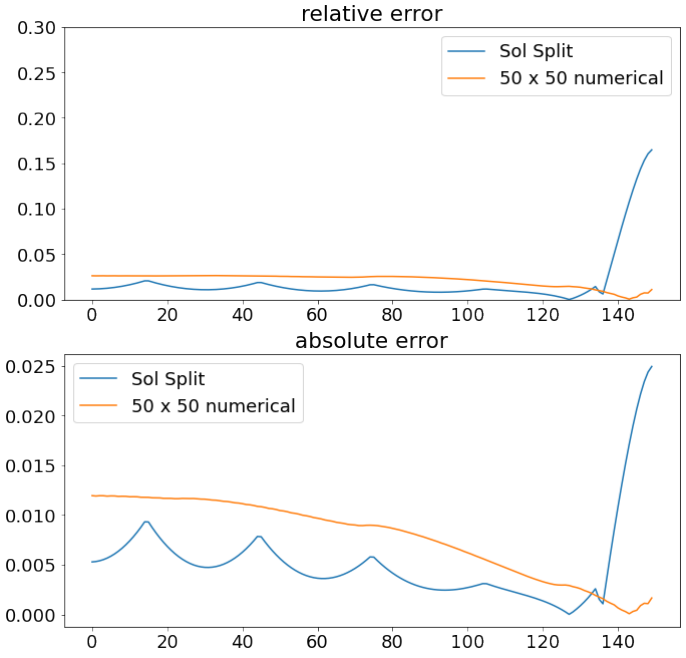

Figure 4: Comparison of the relative error (high) and absolute error (low) when estimating the in flux through the vessel in the Reference and the Split solutions

References

I. Aavatsmark and R. A. Klausen. Well index in reservoir simulation for slanted and slightly curved wells in 3D grids. *SPE Journal*, 8(1):41–48, 2003. ISSN 1086055X. doi: 10.2118/75275-PA.

M. Berg, Y. Davit, M. Quintard, and S. Lorthois. Modelling solute transport in the brain microcirculation: Is it really well mixed inside the blood vessels? *Journal of Fluid Mechanics*, 2019. ISSN 14697645. doi: 10.1017/jfm.2019.866.

Y. Ding and L. Jeannin. A new methodology for singularity modelling in flow simulations in reservoir engineering. *Computational Geosciences*, 5(2):93–119, 2001. ISSN 14200597. doi: 10.1023/A:1013123029671.

I. G. Gjerde, K. Kumar, and J. M. Nordbotten. A singularity removal method for coupled 1D–3D flow models. *Computational Geosciences*, 2019. ISSN 15731499. doi: 10.1007/s10596-019-09899-4.

K. E. Holter, B. Kehlet, A. Devor, T. J. Sejnowski, A. M. Dale, S. W. Omholt, O. P. Ottersen, E. A. Nagelhus, K. A. Mardal, and K. H. Pettersen. Interstitial solute transport in 3D reconstructed neuropil occurs by diffusion rather than bulk flow. *Proceedings of the National Academy of Sciences of the United States of America*, 114(37):9894–9899, 2017. ISSN 10916490. doi: 10.1073/pnas.1706942114.

S. Jayasinghe, D. L. Darmofal, E. Dow, M. C. Galbraith, and S. Allmaras. A discretization-independent distributed well model. *SPE Journal*, 24(6):2946–2967, 2019. ISSN 1086055X. doi: 10.2118/198898-PA.

P. Jenny, S. H. Lee, and H. A. Tchelepi. Multi-scale finite-volume method for elliptic problems in subsurface flow simulation. *Journal of Computational Physics*, 187(1):47–67, 2003. ISSN 00219991. doi: 10.1016/S0021-9991(03)00075-5.

T. Koch, R. Helmig, and M. Schneider. A new and consistent well model for one-phase flow in anisotropic porous media using a distributed source model. *Journal of Computational Physics*, 410:109369, 2020a. ISSN 10902716. doi: 10.1016/j.jcp.2020.109369. URL `https://doi.org/10.1016/j.jcp.2020.109369`.

T. Koch, M. Schneider, R. Helmig, and P. Jenny. Modeling tissue perfusion in terms of 1d-3d embedded mixed-dimension coupled problems with distributed sources. *Journal of Computational Physics*, 410: 109370, 2020b. ISSN 10902716. doi: 10.1016/j.jcp.2020.109370. URL `https://doi.org/10.1016/j.jcp.2020.109370`.

D. W. Peaceman. Interpretation of Well Block Pressures in Numerical Reservoir Simulation. 1978.

M. Peyrounette, Y. Davit, M. Quintard, and S. Lorthois. Multiscale modelling of blood flow in cerebral microcirculation: Details at capillary

scale control accuracy at the level of the cortex. *PLoS ONE*, 13(1):1–35, 2018. ISSN 19326203. doi: 10.1371/journal.pone.0189474. URL http://dx.doi.org/10.1371/journal.pone.0189474.